



Quinone chemistry in respiratory complex I involves protonation of a conserved aspartic acid residue

Caroline Harter¹, Frédéric Melin², Franziska Hoeser¹, Petra Hellwig^{2,3} , Daniel Wohlwend¹ and Thorsten Friedrich¹ 

¹ Institut für Biochemie, Albert-Ludwigs-Universität Freiburg, Germany

² Laboratoire de Bioélectrochimie et Spectroscopie, UMR 7140, CMC, Université de Strasbourg CNRS, Strasbourg, France

³ Institut Universitaire de France (IUF), Paris, France

Correspondence

T. Friedrich, Institut für Biochemie, Albert-Ludwigs-Universität Freiburg, Albertstr. 21, 79104 Freiburg, Germany
Tel: +49 (0)761 203 6060
E-mail: friedrich@bio.chemie.uni-freiburg.de

(Received 5 August 2024, revised 22 August 2024, accepted 23 August 2024, available online 11 September 2024)

doi:10.1002/1873-3468.15013

Edited by Peter Brzezinski

Respiratory complex I is a central metabolic enzyme coupling NADH oxidation and quinone reduction with proton translocation. Despite the knowledge of the structure of the complex, the coupling of both processes is not entirely understood. Here, we use a combination of site-directed mutagenesis, biochemical assays, and redox-induced FTIR spectroscopy to demonstrate that the quinone chemistry includes the protonation and deprotonation of a specific, conserved aspartic acid residue in the quinone binding site (D325 on subunit NuoCD in *Escherichia coli*). Our experimental data support a proposal derived from theoretical considerations that deprotonation of this residue is involved in triggering proton translocation in respiratory complex I.

Keywords: *Escherichia coli*; iron–sulfur cluster; NADH dehydrogenase; NADH:quinone oxidoreductase; proton-coupled electron transfer; quinone reduction; redox-induced FTIR spectroscopy; site-directed mutagenesis

Proton-pumping NADH:ubiquinone oxidoreductase, also called respiratory complex I, is essential for cellular energy metabolism in most organisms. It catalyzes the oxidation of NADH and uses the electrons for quinone (Q) reduction. The redox reaction is coupled with the translocation of protons across the membrane [1–5]. These reactions are spatially separated: A so-called peripheral arm catalyzes electron transfer and a so-called membrane arm is responsible for proton translocation [6–10]. Mitochondrial complex I is made up of 45 different subunits including 14 conserved subunits, which are present in all species that contain a proton-pumping NADH:Q oxidoreductase [1–7]. In general, complex I from bacteria consists of the 14 core subunits. As a special case, the complex from *Escherichia coli* comprises just 13 subunits called NuoA to

NuoN due to the fusion of the genes encoding subunit NuoCD [11,12]. The structure of the 14 core subunits is strictly conserved, so that the complex from *E. coli* represents a minimal structural form of a proton-pumping NADH:Q oxidoreductase [4,6,9,13–17].

NADH is oxidized by flavin mononucleotide (FMN) at the tip of the peripheral arm, and electrons are transferred by a series of iron–sulfur (Fe/S) clusters over a 100 Å distance towards the membrane [1–6]. Here, Q is reduced by the most distal Fe/S cluster N2 (Fig. 1) ~20–30 Å above the membrane plane [1–6]. Q is bound in a unique cavity composed of subunits from both arms. The membrane arm contains four putative proton pathways that are connected to each other and to the Q cavity by an approximately 200 Å long central axis of buried charged residues [4,6,9,13–17,19]. Three proton

Abbreviations

FMN, flavin mononucleotide; Ferricyanide, the hexacyanoferrate anion; Fe/S, iron–sulfur; LMNG, *Lauryl maltose neopentyl glycol*; MD, molecular dynamics; MES, 2-morpholinoethanesulfonic acid; OD, optical density; SDS/PAGE, sodium dodecylsulfate polyacrylamide gel electrophoresis.

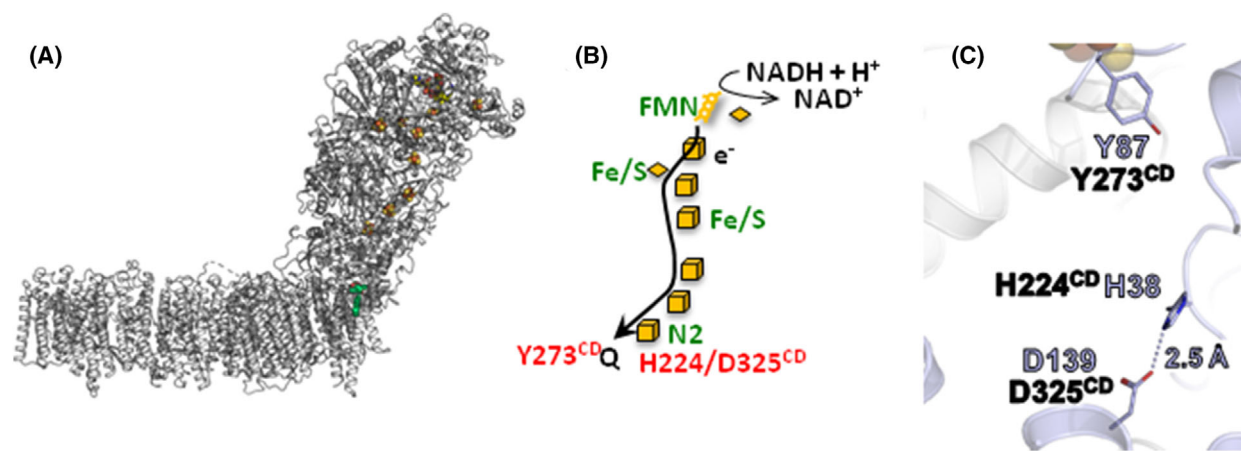


Fig. 1. Structure of and electron transfer in complex I. (A) Structure of *E. coli* complex I (PDB: 7Z7S) with the subunits in gray [18]. The FMN and the Fe/S clusters are depicted in their standard atomic colors. The position of Q in this structure is shown in red and green. (B) Scheme of the electron transfer in the peripheral arm of the complex from NADH (top) to the quinone (bottom). The amino acids mentioned in the text are depicted. (C) Arrangement of the amino acids in question in the Q binding site from *T. thermophilus* complex I (PDB: 4HEA). The Asp/His H-bond is indicated by a dashed line and the distance is provided. The residues are shown in the *T. thermophilus* (purple) and in the *E. coli* (black) numbering. The position of the most distal Fe/S cluster N2 is shown at the top of the figure.

pathways are located on each of subunits NuoL, M and N of the membrane arm. The fourth pathway, called the E-channel [6], is proximal to the Q binding site and it is composed of NuoH, A, J and K [6,18]. Several mechanisms of proton translocation including all or just a few of the putative proton pathways are currently under discussion [5,8–10,18,20–23].

Before the structure of complex I was known, we showed by redox-induced FTIR difference spectroscopy that the potential step from -0.3 to -0.1 V is coupled with the protonation of an acidic amino acid residue [24]. This potential step was attributed to the oxidation-reduction of Fe/S cluster N2 with a redox potential of -0.16 V at pH 6 [25]. As N2 is located on NuoB, we tried to identify the acidic amino acid in question by site-directed mutagenesis of NuoB without a clear result [25]. Electron transfer from N2 to Q is only possible when Q penetrates deeply into its binding cavity in 12 to 10 Å distance from N2 [17,18,20,26,27]. Redox titrations revealed a redox potential of tightly bound Q of less than -300 mV [28,29]. It was suggested that this site corresponds to a so-called low potential binding site ($E_m \sim -0.3$ V) and that Q moves inside its binding cavity to another, the so-called high-potential binding site, where it takes a more positive redox potential (estimated to $E_m \sim 0.08$ V) [23,30].

Structural and biochemical data as well as MD simulations [6,26,31–33] suggested that the carbonyl groups of the quinone headgroup are in hydrogen-bond contact to conserved H224^{CD} and Y273^{CD} (the superscript refers to the name of the *E. coli* subunit; numbering

according to UniProt [34]. The different residue numbers in various organisms are listed in Table S1). The position of H224^{CD} is further stabilized by forming an ion pair with D325^{CD} [6,26]. From large-scale computational simulations, it was concluded that the reduction of Q is coupled with an opening of the His/Asp ion pair and subsequent protonation of reduced Q by Y273^{CD} and H224/D325^{CD} [26]. This would in turn generate a significant charge imbalance that is transmitted to the membrane arm. These steps were discussed as the initial charging steps of proton translocation [26].

We suspected that D325^{CD} could be the acidic amino acid that is protonated during the potential step from -0.3 to -0.1 V [24]. To this end, we generated several mutations at position D325^{CD} in *E. coli* complex I that significantly affect the electron transfer activity without disturbing the assembly of the complex. The sensitivity to the Q-site-specific inhibitor piericidin A is significantly decreased. Redox-induced FTIR spectroscopy of the D325A^{CD} variant clearly shows that this residue is protonated upon electrochemically induced electron transfer. Possible implications for energy coupling in complex I are discussed.

Materials and methods

Strains, plasmids, and oligonucleotides

A derivative of *E. coli* BW25113 [35] chromosomally lacking *ndh* was used to overproduce complex I from a plasmid [36]. Here, the chromosomal *nuo* operon is replaced by a

resistance cartridge (*nptII*). *Escherichia coli* strain DH5 α Δ *nuo* was used for site-directed mutagenesis to avoid recombination [36]. Oligonucleotides were obtained from Sigma-Aldrich. Restriction enzymes were obtained from Thermo Fisher Scientific. Site-directed mutations were introduced into *nuoCD* on plasmid pBAD $_{nuoHis}$ [37] according to the QuikChange protocol (Stratagene, La Jolla, CA, USA). A silent mutation was introduced by PCR using the KOD Hot Start DNA Polymerase (Novagen), generating a new restriction site to identify positive clones by restriction analysis. The primer pairs for site-directed mutagenesis are listed in Table S2. Mutations were examined by DNA sequencing (Eurofins Genomics, Ebersberg, Germany).

Cell growth and preparation of cytoplasmic membranes

To test the functionality of complex I, parental and mutant strains were grown aerobically in minimal medium with 25 mM acetate as sole carbon source [38] at 37 °C while agitating at 180 rpm. Expression of the *nuo* operon was induced by an addition of 0.02% (w/v) L-arabinose. Cell growth was measured as optical density at 600 nm (OD₆₀₀). For protein preparations, cells were grown in rich autoinduction medium with 34 $\mu\text{g}\cdot\text{mL}^{-1}$ chloramphenicol [38] and harvested by centrifugation. The sedimented cells were suspended in a fivefold volume of buffer A (50 mM MES/-NaOH, 50 mM NaCl, pH 6.0) containing 0.1 mM PMSF and a few grains of DNaseI and disrupted by three passages through an HPL-6 (Maximator, 1000–1500 bar) [38]. Cytoplasmic membranes were obtained by differential centrifugation [38] and suspended in an equal volume (1:1, w/v) of buffer A* (buffer A with 5 mM MgCl_2) with 0.1 mM PMSF.

Sucrose gradient centrifugation

Proteins were extracted from the cytoplasmic membrane by an addition of 1% (w/v) LMNG (2,2-didecylpropane-1,3-bis- β -D-maltopyranoside; Anatrace) to a membrane suspension in buffer A* [38]. After incubation for 1 h at 4 °C, the suspension was centrifuged for 20 min at 160 000 *g* and 4 °C (Rotor 60Ti, Sorvall wX+ Ultra Series centrifuge; Thermo Scientific). 0.5 mL supernatant was loaded onto 24 mL gradients of 5–30% (w/v) sucrose in A*_{LMNG} (buffer A* with 0.005% (w/v) LMNG) and centrifuged for 16 h at 104 000 *g* (4 °C, Rotor SW28, Sorvall wX+ Ultra Series centrifuge; Thermo Scientific). The gradients were fractionated into 1 mL portions.

Protein preparation

The D325A^{CD} variant was prepared as described [39]. In short, membrane proteins were extracted with 2% (w/v)

LMNG, the cleared extract was adjusted to 20 mM imidazole and applied to a 35 mL ProBond Ni²⁺-IDA column (Invitrogen, Carlsbad, CA, USA) in binding buffer (A*_{pH6.8} with 0.005% (w/v) LMNG and 20 mM imidazole, pH 6.8). Bound proteins were eluted with binding buffer containing 308 mM imidazole. Fractions with NADH/ferricyanide oxidoreductase activity were pooled, concentrated by ultrafiltration in 100 kDa MWCO Amicon Ultra-15 centrifugal filters (Millipore, Darmstadt, Germany) and applied onto a Superose 6 size-exclusion chromatography column (300 mL; GE Healthcare, Freiburg, Germany) equilibrated in buffer A* with 10% (v/v) glycerol and 0.005% (w/v) LMNG. Fractions with the highest NADH/ferricyanide oxidoreductase activity were used for further studies.

Activity assays

Activity assays were performed at 30 °C. The NADH oxidase activity of cytoplasmic membranes was determined by a Clarke-type oxygen electrode (DW1, Hansatech, Pentney, UK) as described [38]. The electrode was calibrated by an addition of a few grains sodium dithionite to air saturated buffer [40]. NADH oxidase activity was inhibited by an addition of various amounts of piericidin A (ChemCruz, Heidelberg, Deutschland) to the NADH-induced reaction. The NADH/ferricyanide oxidoreductase activity was determined as decrease of the ferricyanide absorbance at 410 nm [38] with a diode-array spectrometer (QS cuvette, *d* = 1 cm, Hellma; TIDAS S, J&M, Aalen, Germany) using an ϵ of 1 $\text{mm}^{-1}\cdot\text{cm}^{-1}$ [41]. The NADH:decyl-Q oxidoreductase activity was measured as decrease of the NADH concentration at 340 nm using an ϵ of 6.3 $\text{mm}^{-1}\cdot\text{cm}^{-1}$ (QS cuvette, *d* = 1 cm, Hellma; TIDAS S, J&M Aalen). The assay contained 60 μM decyl-Q, 2 μg complex I or the D325A^{CD} variant and a tenfold molar excess (5 μg) *E. coli* cytochrome *bo*₃ oxidase in buffer A*_{LMNG}. The reaction was started by an addition of 150 μM NADH [38].

IR spectroscopy

The experiments were performed in a thin-layer transmission electrochemical cell as previously described [42,43]. The semi-transparent gold grid that serves as a working electrode was modified with 1:1 solution of cysteamine and mercaptopropionic acid (mixture of positively and negatively charged thiols) in order to prevent the adsorption of protein on the electrode surface. A platinum contact and an aqueous Ag/AgCl 3 M KCl electrode were used as counter and reference electrodes, respectively. An hour before each experiment the protein was incubated with a cocktail of 19 mediators with a final concentration of 25 μM [44]. The cell was assembled as described previously [24]. The oxidized minus reduced FTIR difference spectra were obtained in the –300/–500 mV vs Ag/AgCl potential range

(the values are converted to SHE' potentials by adding +208 mV) using a Vertex 70 FTIR spectrometer from Bruker Optics, with an equilibration time of 5 min for each step. The redox reaction was cycled over 50–80 times and for each redox state two spectra (256 scans, 4 cm⁻¹ resolution) were averaged.

Other analytical methods

Protein concentration was determined by the biuret method using BSA as a standard [45]. The concentration of purified complex I was determined by UV/vis-spectroscopy (TIDAS S; J&M) using an ϵ_{280} of 781 mm⁻¹ cm⁻¹ as derived from the amino acid sequence [46]. SDS/PAGE (sodium dodecyl sulfate/polyacrylamide gel electrophoresis) was performed with a 10% separating gel and a 3.9% stacking gel [47]. The pKa of D325^{CD} was calculated with PropKa3 [48] using the pdb model 7Z7S of *E. coli* complex I [18].

Results

D325^{CD} of *E. coli* complex I was individually mutated to A, E, N and Q by changing the respective codon on the pBAD_{nuo}_{His} expression plasmid that encodes the entire *E. coli nuo* operon under the control of the inducible P_{BAD} arabinose promoter [37]. The expression strain BW25113 Δ *ndh nuo:nptII_FRT* was transformed with plasmids either encoding the original *nuo*-genes or the corresponding mutations. Due to the lack of the alternative NADH dehydrogenase (*ndh*) [38] and the chromosomally encoded complex I, all NADH-induced activities of membranes from this strain exclusively derive from complex I and the variants encoded on the plasmid.

To screen for an effect of the mutations on complex I, the host strain individually transformed with the various plasmids was grown in minimal medium with acetate as non-fermentable carbon source. Here, an intact complex I is required for fast growth to high OD values [38]. The mutant strains D325A^{CD} and D325E^{CD} grew as fast as the parental strain. Only the D325N^{CD} and D325Q^{CD} mutant strains grew slightly slower (Fig. 2). This already suggests that complex I is fully assembled and active in the A and E mutants, while it may have a decreased activity in the N and Q mutants.

The assembly of the complex I variants in the mutant strains was assessed by separating proteins extracted from cytoplasmic membranes with LMNG using sucrose gradient centrifugation (Fig. 2). The position of the complex and the variant proteins in the gradient was determined by their NADH/ferricyanide oxidoreductase activity. Parental complex I sediments around fraction 16 as expected [49]. The

variants sedimented at the same position of the gradient with approximately the same total activity (Fig. 2) indicating a similar amount of protein in the mutant membranes. As an exception, the strain producing the D325A^{CD} variant shows a significantly higher total activity than the parental strain (Fig. 2).

The amount of the complex and the variants in cytoplasmic membranes was also determined by measuring the NADH/ferricyanide oxidoreductase activity (Table 1). This activity is mediated by FMN bound to NuoF and is not coupled to Q reduction or proton pumping. The activity of the D325A^{CD} mutant strain is significantly higher than that of the parental strain, while that of the D325E^{CD} and D325Q^{CD} mutant strains is slightly diminished. The NADH/ferricyanide oxidoreductase activity of the D325N^{CD} mutant membranes is only two thirds of that of the parental strain. These results are in good agreement with the activity profiles of the sucrose gradients (Fig. 2). For unknown reasons, the D325A^{CD} mutant produces more of the variant than the parent strain of complex I. The physiological activity of complex I was determined by measuring the NADH oxidase activity of cytoplasmic membranes. In this assay, NADH is oxidized by complex I and the produced quinol is used by the quinol oxidases to reduce oxygen to water. The decrease of the oxygen concentration in the buffer is measured. Here, the D325A^{CD} mutant strain showed a slightly diminished activity while that of the other mutant strains was half and one third of the parental strain, respectively (Table 1). Production of complex I from the *nuo*-plasmids might lead to different amounts of the complex in the strains. To compensate for this difference, the NADH oxidase activity was normalized for the amount of complex I in the respective membranes as derived from the NADH/ferricyanide oxidoreductase activity (Table 1). Taking the different amount of complex I in the membrane into account, the D325A^{CD} and D325E^{CD} mutant strains exhibited about 60% and the other strains approximately half of the activity of the parental strain (Table 1). Thus, the mutations clearly diminished complex I electron transfer activity without blocking the reaction. This is in agreement with previous reports [26,50]. The rapid growth of the mutant strain producing the D325A^{CD} variant (Fig. 2) is explained by the fact that although the variant retains 62% of its physiological activity, this is compensated for by the production of 132% of the amount of the variant.

To determine the influence of the mutation on inhibitor binding, the NADH oxidase activity was titrated with piericidin A, a specific Q site inhibitor of complex I [40]. The IC₅₀ for the parental membranes was 3.3 μ M piericidin A (Table 2), which is in good

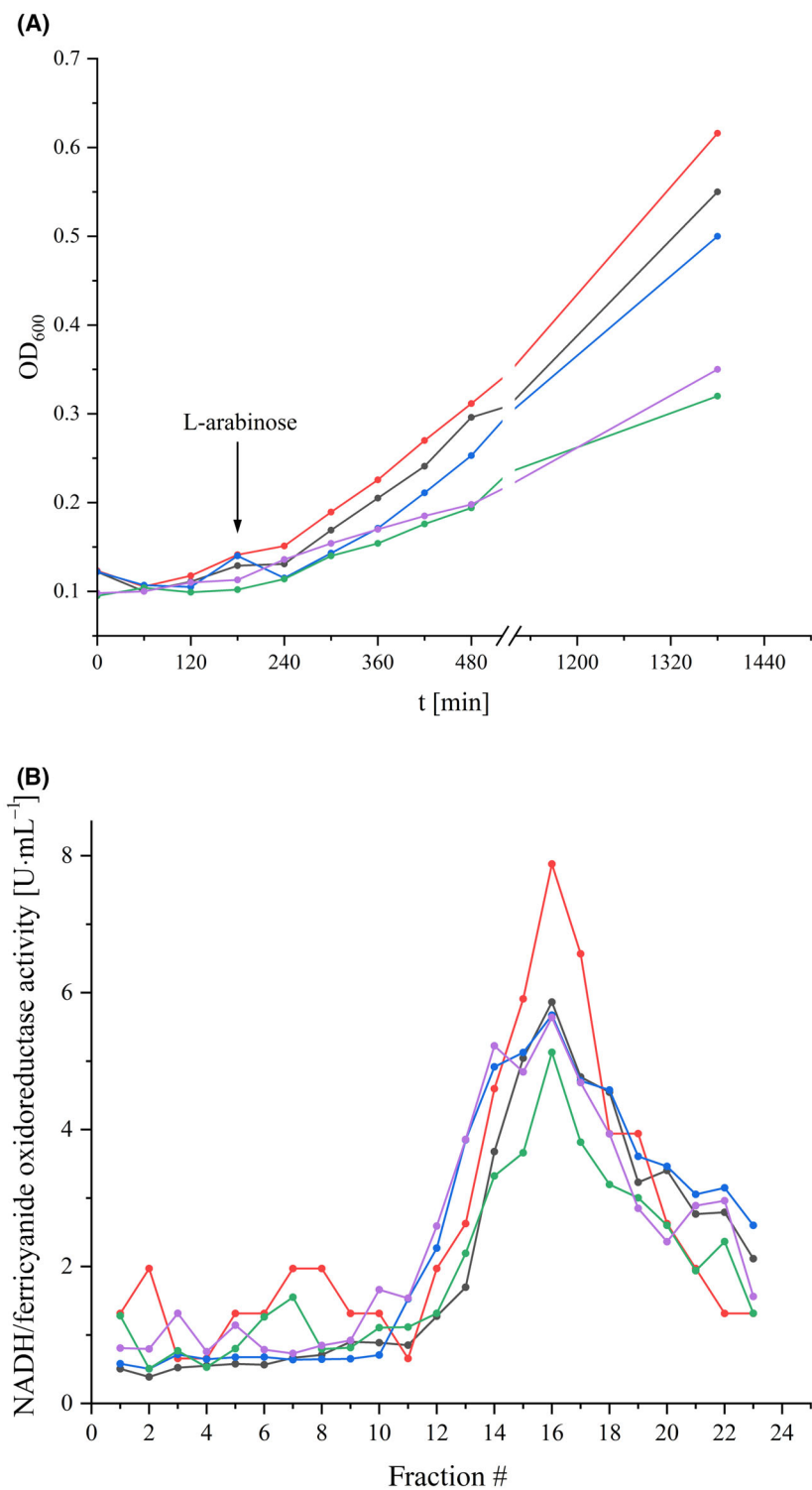


Fig. 2. Growth of the *nuoCD* mutant strains and stability of the variants. (A) Growth curves of the reference strain producing parental complex I (black) and the D325^{CD} mutant strains D325A^{CD} (red), D325E^{CD} (blue), D325N^{CD} (green), and D325Q^{CD} (violet) in minimal medium with acetate as the only carbon source. The arrow marks the induction of gene expression with 0.02% (w/v) L-arabinose. (B) Sucrose gradients of detergent solubilized membranes from the parental strain (black) and the *nuoCD* mutant strains D325A^{CD} (red), D325E^{CD} (blue), D325N^{CD} (green) and D325Q^{CD} (violet). The NADH/ferricyanide oxidoreductase activity of each fraction is shown; the activities are normalized to 20 mg protein applied on each gradient.

Table 1. NADH oxidase and NADH/ferricyanide oxidoreductase activity of cytoplasmic membranes from *E. coli* parental strain (WT) and D325^{CD} mutant strains. Data were obtained from three measurements of two biological replicates, the standard deviation is given.

Strain	NADH/ferricyanide oxidoreductase activity		NADH oxidase activity		Normalized NADH oxidase activity	
	(U·mg ⁻¹ total protein)	(%)	(U·mg ⁻¹ total protein)	(%)	(U·mg ⁻¹ total protein)	(%)
WT	2.9 ± 0.2	100 ± 5	0.51 ± 0.02	100 ± 7	0.51 ± 0.05	100 ± 9
D325A ^{CD}	3.8 ± 0.3	132 ± 9	0.41 ± 0.01	81 ± 3	0.32 ± 0.03	62 ± 10
D325E ^{CD}	2.7 ± 0.2	92 ± 9	0.28 ± 0.02	55 ± 9	0.30 ± 0.03	59 ± 10
D325N ^{CD}	1.9 ± 0.3	64 ± 18	0.16 ± 0.03	31 ± 23	0.26 ± 0.06	50 ± 28
D325Q ^{CD}	2.3 ± 0.2	80 ± 10	0.17 ± 0.03	33 ± 21	0.22 ± 0.04	43 ± 22

Table 2. Inhibition of the NADH oxidase activity of cytoplasmic membranes from *E. coli* parental and *nuoCD* mutant strains. Data were obtained from two measurements of three biological replicates, the standard deviation is given.

Strain	IC ₅₀ (piericidin A) (μM)
WT	3.5 ± 0.2
D325A ^{CD}	9.3 ± 0.8
D325E ^{CD}	6.2 ± 0.5
D325N ^{CD}	17.4 ± 0.6
D325Q ^{CD}	16.9 ± 1.2

agreement with previous data [40]. Remarkably, all D325^{CD} mutants showed a significantly lower affinity to piericidin A. The D325E^{CD} mutant strain that contains a longer acidic side chain exhibits an approximately two-fold and membranes from the D325A^{CD} mutant strain an approximately three-fold higher IC₅₀ (Table 2). Membranes from the mutants with an amide at this position, D325Q^{CD} and D325N^{CD}, show high IC₅₀ values of around 17 μM (Table 2). The latter indicates a disturbed binding of piericidin A at its binding site. This is in agreement with structural data indicating that H224^{CD}, the ion-pair binding partner of D325^{CD}, is strongly involved in specific binding of piericidin A [16].

To clarify whether D325^{CD} is the acidic amino acid residue that we identified to be protonated by the potential step from -0.3 to -0.1 V [24], complex I and the D325A^{CD} variant were prepared to homogeneity by affinity and size-exclusion chromatography (Fig. S1). The D325A^{CD} variant was selected for comparison as the methyl protons show no signals in the region from 1800 to 1710 cm⁻¹. From 50 g cells 7–10 mg of complex I and of the variant protein were obtained. The elution profiles and the SDS-gel of the preparations of complex I and the variant show no

significant differences (Fig. S1). The specific NADH/ferricyanide oxidoreductase activity of preparations of the D325A^{CD} variant is 98 ± 3.5 U·mg⁻¹ of the variant and thus, similar to that of complex I with 105 ± 2.8 U·mg⁻¹ of complex I. Likewise, the variant showed about 61% (17.2 ± 0.4 U·mg⁻¹ of the variant) of the specific NADH:decyl-Q oxidoreductase activity of the parental complex (28.2 ± 2.4 U·mg⁻¹ of complex I), which is in line with data obtained from membranes (Table 1). The NADH:decyl-Q oxidoreductase activity of the isolated enzymes is used to measure electron transfer from NADH to the artificial substrate decyl-Q, whereby the electrons follow the physiological path *via* the FMN and the FeS clusters to the Q binding site. The reaction is coupled with proton translocation, but this has no effect on the assay as the enzyme is not reconstituted in proteoliposomes.

The redox-dependent reorganizations of complex I and the contributions of titratable amino acid residues have been described by infrared spectroscopy [24]. The ν(C=O) modes of protonated aspartic and glutamic acid side chains contribute in the spectral range from 1800 to 1710 cm⁻¹. This spectral region is highly characteristic for protonated acidic amino acid residues in membrane proteins [51,52]. The spectra were recorded under the same experimental conditions as reported [24]. Accordingly, a potential step from -0.3 to -0.1 V was applied to both samples. In this range, tightly bound Q will be reduced and protonated and it will move away from its tight position in the cavity in proximity of N2 [23,30]. Spectra of the complex and the variant were recorded from 1800 to 1200 cm⁻¹ as in our original experiment (Fig. 3). The individual signals present in the redox difference spectra of complex I have already been discussed in detail [24]. Noteworthy, the spectra look highly similar to those obtained with the preparation of the chromosomally encoded complex in a different detergent [24]. The complex I difference spectra feature a clear signal at 1711 cm⁻¹

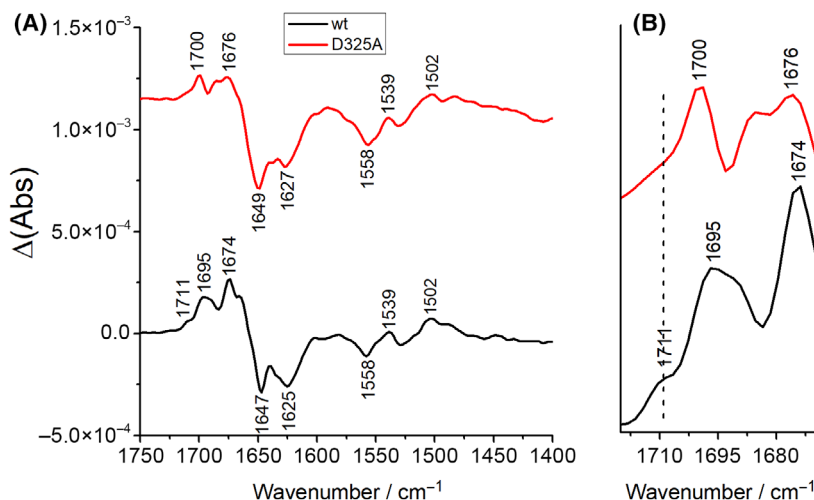


Fig. 3. (A) Oxidized minus reduced FTIR difference spectra of the complex I and the D325A^{CD} variant at pH 6 in the $-0.3/-0.1$ V potential range. (B) Magnified view of the $1720\text{--}1670$ cm^{-1} spectral range.

as reported for the previously published preparation (Fig. 3). This signal contains contributions from the FMN and another group that was originally attributed to an acidic amino acid side chain due to its clearly lower intensity in the spectra of the NADH dehydrogenase fragment of the complex that contains the FMN but lacks cluster N2 and the Q binding site [24]. Comparison of redox difference spectra of complex I and the D325A^{CD} variant reveals that the signal at 1711 cm^{-1} is nearly lost in the redox difference spectrum of the D325A^{CD} variant (Fig. 3). Following our previous findings [24] the very low residual absorbance is attributed to the FMN. Since both spectra were recorded in a pH 6 buffer, the pKa of the residue in question should be higher than 6. Only a few acidic amino acid residues of complex I are predicted to have a pKa above 6 by using the PropKa3 software. According to these predictions, the pKa of D325^{CD}, the aspartic acid residue that is the focus of our study, fulfills this requirement with a pKa of 8.3, which is consistent with the experimental data. Taking all experimental evidence together our data strongly suggest that this D325^{CD} becomes deprotonated upon Q reduction at -0.3 V and protonated when the reduced and protonated QH₂ moves away from N2 to another position in the Q cavity at -0.1 V.

Discussion

Mutation of D325^{CD} to A, E, N, and Q does not hamper the assembly of the complex (Fig. 2). However, these mutations clearly diminish the NADH:Q oxidoreductase activity normalized to the amount of the

protein in the membrane (Table 1) in agreement with previous studies on the *E. coli* enzyme [26,50]. As the mutations do not fully block activity, D325^{CD} is not essential for the enzyme's activity. In contrast, based on the FTIR spectroscopic data, D325^{CD} clearly is the amino acid residue that is deprotonated when the complex experiences a potential of -0.3 V and protonated at a potential of -0.1 V (Fig. 3).

There is a general agreement that Q is reduced by electron transfer from the most distal Fe/S cluster N2, when bound to the tight position in the Q binding cavity of complex I (Fig. 1) [1–10]. Most likely, Q is fully reduced to Q²⁻ [26] that readily accepts protons from nearby donors. However, it is unclear whether Q²⁻ is fully protonated at this position resulting in QH₂ or whether a quinol anion QH⁻ is formed instead [53]. Furthermore, the proton source is still under debate. From co-crystallization of the *Thermus thermophilus* complex I with piericidin A and the substrate analog decyl-Q, Baradaran *et al.* concluded that one of the redox-active carbonyl groups interacts with Y273^{CD} and the other one with H224^{CD} (*E. coli* numbering, see Table S1) [6]. The same conserved Y273^{CD} and H224^{CD} residues were also identified by molecular dynamics (MD) simulations as obligate binding partners to enable redox-driven proton translocation [23,32,33,54,55]. However, so far no structure has been solved in which the carbonyl groups of a long-chain Q are bound by these two residues. Furthermore, biochemical data obtained with *Y. lipolytica* complex I indicate that these two residues might just ligate the two carbonyl groups to enable a proper positioning of the Q headgroup for electron transfer. Mutagenesis of these residues prevented the reaction with long-chain

Qs such as the native Q₉, however, the isolated variants were fully active with short-chain quinones such as Q₁ and Q₂ [31]. This could mean that these residues may not be involved in the protonation of the Q [16,31].

H224^{CD} forms an ion pair with D325^{CD} that was proposed to open upon Q reduction and protonation, thus leading to deprotonation of D325^{CD} by H224^{CD} [26]. Our FTIR data show that the deprotonated carboxylate of D325^{CD} is found in the reduced state at -0.3 V and that this side chain becomes protonated to a neutral carboxylic acid in the oxidized state at -0.1 V (Fig. 3). At -0.3 V, the potential at which Q is reduced, D325^{CD} is therefore present in the deprotonated form. According to MD simulations, D325^{CD} becomes deprotonated as soon as Q is reduced to the Q²⁻ state by electron transfer from cluster N2 [26]. Q²⁻ is rapidly protonated to QH₂ from a yet unknown source, which could be the nearby conserved Y273^{CD} and H224^{CD} residues as discussed above [26]. According to quantum mechanics/molecular mechanics simulations, deprotonation of D325^{CD} upon QH₂ formation is accomplished by H224^{CD}. Thus, our FTIR difference spectra fully support this suggestion (Fig. 3). Following the simulations [26], the anionic D325^{CD} moves away from H224^{CD} towards the membrane arm. This is enabled by D325^{CD} being part of a conformationally flexible four-helix bundle [6]. The movement of the anionic D325^{CD} should induce conformational changes that are involved in driving proton translocation in the membrane arm [26]. Remarkably, the D325N^{CD} variant was shown to be able to translocate protons. This was explained by the fact that this residue is part of a larger proton relay system [26].

Beyond the scope of the MD simulations, our experimental data now show that when QH₂ moves from its low potential to its high-potential position in the cavity at -0.1 V, D325^{CD} becomes protonated, most likely after proton translocation in the membrane arm. The proton may derive from the electric ‘back-wave’ in the membrane arm [23] or the charge re-distribution in the membrane arm upon proton uptake from the cytosol [18]. Thus, we experimentally confirm the proposal that D325^{CD} is in the deprotonated state during Q reduction [26] and show that it is in the protonated state when QH₂ moves to its high-potential binding site.

Acknowledgements

This work was supported by the Deutsche Forschungsgemeinschaft (DFG) by grants 278002225/RTG 2202 and SPP1927; FR 1140/11-2 to TF and ANR-10-LABX-0026_CSC to PH. Open Access funding enabled and organized by Projekt DEAL.

Author contributions

CH and FH constructed the expression plasmids, purified the proteins, performed the biochemical experiments and acquired the biochemical data, FM and PH recorded the FTIR spectra, CH, FM, FH, PH, and TF analyzed the data, DW performed pK_a calculations, TF wrote the manuscript with contributions from all authors, TF designed the study.

Peer review

The peer review history for this article is available at <https://www.webofscience.com/api/gateway/wos/peer-review/10.1002/1873-3468.15013>.

Data accessibility

The data supporting the findings of this article are available from the corresponding author upon reasonable request.

References

- 1 Hirst J (2013) Mitochondrial complex I. *Annu Rev Biochem* **82**, 551–575.
- 2 Friedrich T (2014) On the mechanism of respiratory complex I. *J Bioenerg Biomembr* **46**, 255–269.
- 3 Sazanov LA (2015) A giant molecular proton pump: structure and mechanism of respiratory complex I. *Nat Rev Mol Cell Biol* **16**, 375–388.
- 4 Parey K, Wirth C, Vonck J and Zickermann V (2020) Respiratory complex I – structure, mechanism and evolution. *Curr Opin Struct Biol* **63**, 1–9.
- 5 Kaila VRI (2021) Resolving chemical dynamics in biological energy conversion: long-range proton-coupled electron transfer in respiratory complex I. *Acc Chem Res* **54**, 4462–4473.
- 6 Baradaran R, Berrisford JM, Minhas GS and Sazanov LA (2013) Crystal structure of the entire respiratory complex I. *Nature* **494**, 443–448.
- 7 Gnannt E, Dörner K, Stramprecht MFJ, de Vries S and Friedrich T (2016) The multitude of iron-sulfur clusters in respiratory complex I. *Biochim Biophys Acta* **1857**, 1068–1072.
- 8 Cabrera-Orefice A, Yoga EG, Wirth C, Siegmund K, Zwicker K, Guerrero-Castillo S, Zickermann V, Hunte C and Brandt U (2018) Locking loop movement in the ubiquinone pocket of complex I disengages the proton pumps. *Nat Commun* **9**, 4500.
- 9 Grba D, Chung I, Bridges HR, Agip A-NA and Hirst J (2023) Investigation of hydrated channels and proton pathways in a high-resolution cryo-EM structure of mammalian complex I. *Sci Adv* **9**, eadi1359.

- 10 Kim H, Saura P, Pöwerlein MC, Gamiz-Hernandez AP and Kaila VRI (2023) Quinone catalysis modulates proton transfer reactions in the membrane domain of respiratory complex I. *J Am Chem Soc* **145**, 17075–17086.
- 11 Weidner U, Geier S, Ptock A, Friedrich T, Leif H and Weiss H (1993) The gene locus of the proton-translocating NADH:ubiquinone oxidoreductase in *Escherichia coli*. Organization of the 14 genes and relationship between the derived proteins and subunits of the mitochondrial complex I. *J Mol Biol* **233**, 109–122.
- 12 Braun M, Bungert S and Friedrich T (1998) Characterization of the overproduced NADH dehydrogenase fragment of the NADH:ubiquinone oxidoreductase (complex I) from *Escherichia coli*. *Biochemistry* **37**, 1861–1867.
- 13 Agip A-NA, Blaza JN, Fedor JG and Hirst J (2019) Mammalian respiratory complex I through the lens of Cryo-EM. *Annu Rev Biophys* **48**, 165–184.
- 14 Fiedorczuk K, Letts JA, Degliesposti G, Kaszuba K, Skehel M and Sazanov LA (2016) Atomic structure of the entire mammalian respiratory complex I. *Nature* **538**, 406–410.
- 15 Galemou Yoga E, Angerer H, Parey K and Zickermann V (2020) Respiratory complex I – mechanistic insights and advances in structure determination. *Biochim Biophys Acta* **1861**, 148153.
- 16 Bridges HR, Fedor JG, Blaza NJ, Di Luca A, Jussupow A, Jarman OD, Wright JJ, Agip A-NA, Gamiz-Hernandez AP, Roessler MM *et al.* (2020) Structure of inhibitor-bound mammalian complex. *Nat Commun* **11**, 5261.
- 17 Zheng W, Chai P, Zhu J and Zhang K (2024) High-resolution in situ structures of mammalian respiratory supercomplexes. *Nature* **631**, 232–239.
- 18 Kravchuk V, Petrova O, Kampjut D, Wojciechowska-Bason A, Breese Z and Sazanov L (2022) A universal coupling mechanism of respiratory complex I. *Nature* **609**, 808–814.
- 19 Di Luca A, Gamiz-Hernandez AP and Kaila VRI (2017) Symmetry-related proton transfer pathways in respiratory complex I. *Proc Natl Acad Sci USA* **114**, E6314–E6321.
- 20 Kampjut D and Sazanov L (2020) The coupling mechanism of mammalian respiratory complex I. *Science* **370**, eabc4209.
- 21 Laube E, Meier-Credo J, Langer JD and Kühlbrandt W (2022) Conformational changes in mitochondrial complex I of the thermophilic eukaryote *Chaetomium thermophilum*. *Sci Adv* **8**, eadc 9952.
- 22 Kaila VRI and Wikström M (2021) Architecture of bacterial respiratory chains. *Nat Rev Microbiol* **19**, 319–330.
- 23 Kaila VRI (2018) Long-range proton-coupled electron transfer in biological energy conversion: towards mechanistic understanding of respiratory complex I. *J R Soc Interface* **15**, 20170916.
- 24 Hellwig P, Scheide D, Bungert S, Mäntele W and Friedrich T (2000) FT-IR spectroscopic characterization of NADH:ubiquinone oxidoreductase (complex I) from *Escherichia coli*: oxidation of FeS cluster N2 is coupled with the protonation of an aspartate or glutamate side chain. *Biochemistry* **39**, 10884–10891.
- 25 Flemming D, Hellwig P, Lepper S, Kloer DP and Friedrich T (2006) Catalytic importance of acidic amino acids on subunit NuoB of the *Escherichia coli* NADH:ubiquinone oxidoreductase (complex I). *J Biol Chem* **281**, 24781–24789.
- 26 Sharma V, Belevich G, Gamiz-Hernandez AP, Róg T, Vattulainen I, Verkhovskaya ML, Wikström M, Hummer G and Kaila VRI (2015) Redox-induced activation of the proton pump in the respiratory complex I. *Proc Natl Acad Sci USA* **112**, 11571–11576.
- 27 Chung I, Wright JJ, Bridges HR, Ivanov BS, Biner O, Pereira CS, Arantes GM and Hirst J (2022) Cryo-EM structures define ubiquinone-10 binding to mitochondrial complex I and conformational transitions accompanying Q-site occupancy. *Nat Commun* **13**, 2758.
- 28 Verkhovskiy M, Bloch DA and Verkhovskaya M (2012) Tightly-bound ubiquinone in the *Escherichia coli* respiratory complex I. *Biochim Biophys Acta* **1817**, 1550–1556.
- 29 Verkhovskaya M and Wikström M (2014) Oxidoreduction properties of bound ubiquinone in complex I from *Escherichia coli*. *Biochim Biophys Acta* **1837**, 246–250.
- 30 Wikström M, Sharma V, Kaila VRI, Hosler JP and Hummer G (2015) New perspectives on proton pumping in cellular respiration. *Chem Rev* **115**, 2196–2221.
- 31 Tocilescu MA, Fendel U, Zwicker K, Kerscher S and Brandt U (2007) Exploring the ubiquinone binding cavity of respiratory complex I. *J Biol Chem* **282**, 29514–29520.
- 32 Warnau J, Sharma V, Gamiz-Hernandez AP, Di Luca A, Haapanen O, Vattulainen I, Wikström M, Hummer G and Kaila VRI (2018) Redox-coupled quinone dynamics in the respiratory complex I. *Proc Natl Acad Sci USA* **115**, E8413–E8420.
- 33 Gamiz-Hernandez AP, Jussupow A, Johansson MP and Kaila VRI (2017) Terminal electron-proton transfer dynamics in the quinone reduction of respiratory complex I. *J Am Chem Soc* **139**, 16282–16288.
- 34 The UniProt Consortium (2023) UniProt: the universal protein knowledgebase in 2023. *Nucleic Acids Res* **51**, D523–D531.
- 35 Datsenko KA and Wanner BL (2000) One-step inactivation of chromosomal genes in *Escherichia coli* K-12 using PCR products. *Proc Natl Acad Sci USA* **97**, 6640–6645.

- 36 Burschel S, Kreuzer Decovic D, Nuber F, Stiller M, Hofmann M, Zupok A, Siemiatkowska B, Gorka M, Leimkühler S and Friedrich T (2019) Iron-sulfur cluster carrier proteins involved in the assembly of *Escherichia coli* NADH:ubiquinone oxidoreductase (complex I). *Mol Microbiol* **111**, 31–45.
- 37 Pohl T, Uhlmann M, Kaufenstein M and Friedrich T (2007) Lambda red-mediated mutagenesis and efficient large scale affinity purification of the *Escherichia coli* NADH:ubiquinone oxidoreductase (complex I). *Biochemistry* **46**, 10694–10702.
- 38 Nuber F, Schimpf J, di Rago J-P, Tribouillard-Tanvier D, Procaccio V, Martin-Negrier M-L, Trimouille A, Biner O, von Ballmoos C and Friedrich T (2021) Biochemical consequences of two clinically relevant ND-gene mutations in *Escherichia coli* respiratory complex I. *Sci Rep* **11**, 12641.
- 39 Schimpf J, Oppermann S, Gerasimova T, Santos Seica AF, Hellwig P, Grishkovskaya I, Wohlwend D, Haselbach D and Friedrich T (2022) Structure of the peripheral arm of a minimalistic respiratory complex I. *Structure* **30**, 80–94.e4.
- 40 Friedrich T, van Heek P, Leif H, Ohnishi T, Forche E, Kunze B, Jansen R, Trowitzsch-Kienast W, Höfle G, Reichenbach H *et al.* (1994) Two binding sites of inhibitors in NADH: ubiquinone oxidoreductase (complex I). Relationship of one site with the ubiquinone-binding site of bacterial glucose:ubiquinone oxidoreductase. *Eur J Biochem* **219**, 691–698.
- 41 Friedrich T, Hofhaus G, Ise W, Nehls U, Schmitz B and Weiss H (1989) A small isoform of NADH: ubiquinone oxidoreductase (complex I) without mitochondrially encoded subunits is made in chloramphenicol-treated *Neurospora crassa*. *Eur J Biochem* **180**, 173–180.
- 42 Moss D, Nabedryk E, Breton J and Mäntele W (1990) Redox-linked conformational changes in proteins detected by a combination of infrared spectroscopy and protein electrochemistry. Evaluation of the technique with cytochrome *c*. *Eur J Biochem* **187**, 565–572.
- 43 Melin F and Hellwig P (2020) Redox properties of the membrane proteins from the respiratory chain. *Chem Rev* **120**, 10244–10297.
- 44 Hellwig P, Behr J, Ostermeier C, Richter O-MH, Pfitzner U, Odenwald A, Ludwig B, Michel H and Mäntele W (1998) Involvement of glutamic acid 278 in the redox reaction of the cytochrome *c* oxidase from *Paracoccus denitrificans* investigated by FT-IR spectroscopy. *Biochemistry* **37**, 7390–7399.
- 45 Gornall AG, Bardawill CJ and David MM (1949) Determination of serum proteins by means of the biuret reaction. *J Biol Chem* **177**, 751–766.
- 46 Gill SC and von Hippel PH (1989) Calculation of protein extinction coefficients from amino acid sequence data. *Anal Biochem* **182**, 319–326.
- 47 Schagger H and von Jagow G (1987) Tricine-sodium dodecyl sulfate-polyacrylamide gel electrophoresis for the separation of proteins in the range from 1 to 100 kDa. *Anal Biochem* **166**, 368–379.
- 48 Olsson MHM, Sondergaard CR, Rostkowski M and Jensen JH (2011) PROPKA3: consistent treatment of internal and surface residues in empirical pKa predictions. *J Chem Theory Comput* **7**, 525–537.
- 49 Leif H, Sled VD, Ohnishi T, Weiss H and Friedrich T (1995) Isolation and characterization of the proton-translocating NADH:ubiquinone oxidoreductase from *Escherichia coli*. *Eur J Biochem* **230**, 538–548.
- 50 Sinha PK, Castro-Guerrero N, Patki G, Sato M, Torres-Bacete J, Sinha S, Miyoshi H, Matsuno-Yagi A and Yagi T (2015) Conserved amino acid residues of the NuoD segment important for structure and function of *Escherichia coli* NDH-1 (complex I). *Biochemistry* **54**, 753–764.
- 51 Hellwig P, Barquera B and Gennis RB (2001) Direct evidence for the protonation of aspartate-75, proposed to be at a quinol binding site, upon reduction of cytochrome *bo*₃ from *Escherichia coli*. *Biochemistry* **40**, 1077–1082.
- 52 Zscherp C, Schlessinger R, Titor J, Oesterhelt D and Heberle J (1999) *In situ* determination of transient pKa changes of internal amino acids of bacteriorhodopsin by using time-resolved attenuated total reflection Fourier-transform infrared spectroscopy. *Proc Natl Acad Sci USA* **96**, 5496–5503.
- 53 Djurabekova A, Lasham J, Zdorevskiy O, Zickermann V and Sharma V (2024) Long-range electron proton coupling in respiratory complex I – insights from molecular simulations of the quinone chamber and antiporter-like subunits. *Biochem J* **481**, 499–514.
- 54 Röpke M, Riepl D, Saura P, Di Luca A, Mühlbauer ME, Jussupow A, Gamiz-Hernandez AP and Kaila VRI (2021) Deactivation blocks proton pathways in the mitochondrial complex I. *Proc Natl Acad Sci USA* **118**, e2019498118.
- 55 Teixeira MH and Arantes GM (2019) Balanced internal hydration discriminates substrate binding to respiratory complex I. *Biochim Biophys Acta* **1860**, 541–548.

Supporting information

Additional supporting information may be found online in the Supporting Information section at the end of the article.

Fig. S1. Preparation of complex I and the D325ACD variant.

Table S1. Nomenclature of individual NuoCD positions in various organisms.

Table S2. Oligonucleotides used for site-directed mutagenesis.